



# Redox-controlled carbon and phosphorus burial: A mechanism for enhanced organic carbon sequestration during the PETM



Nemanja Komar\*, Richard E. Zeebe

University of Hawaii, Oceanography Department, Honolulu, HI 96822, USA

## ARTICLE INFO

### Article history:

Received 13 January 2017

Received in revised form 13 July 2017

Accepted 2 September 2017

Available online xxxx

Editor: H. Stoll

### Keywords:

PETM

carbon sequestration

carbon cycle

phosphorus

oxygen

methane hydrate

## ABSTRACT

Geological records reveal a major perturbation in carbon cycling during the Paleocene–Eocene Thermal Maximum (PETM, ~56 Ma), marked by global warming of more than 5 °C and a prominent negative carbon isotope excursion of at least 2.5‰ within the marine realm. The entire event lasted about 200,000 yr and was associated with a massive release of light carbon into the ocean–atmosphere system over several thousands of years. Here we focus on the terminal stage of the PETM, during which the ocean–atmosphere system rapidly recovered from the carbon cycle perturbation. We employ a carbon-cycle box model to examine the feedbacks between surface ocean biological production, carbon, oxygen, phosphorus, and carbonate chemistry during massive CO<sub>2</sub> release events, such as the PETM. The model results indicate that the redox-controlled carbon–phosphorus feedback is capable of producing enhanced organic carbon sequestration during large carbon emission events. The locale of carbon oxidation (ocean vs. atmosphere) does not affect the amount of carbon sequestered. However, even though the model produces trends consistent with oxygen, excess accumulation rates of organic carbon (~1700 Pg C during the recovery stage), export production and δ<sup>13</sup>C data, it fails to reproduce the magnitude of change of sediment carbonate content and the CCD over-deepening during the recovery stage. The CCD and sediment carbonate content overshoot during the recovery stage is muted by a predicted increase in CaCO<sub>3</sub> rain. Nonetheless, there are indications that the CaCO<sub>3</sub> export remained relatively constant during the PETM. If this was indeed true, then an initial pulse of 3,000 Pg C followed by an additional, slow leak of 2,500 Pg C could have triggered an accelerated nutrient supply to the surface ocean instigating enhanced organic carbon export, consequently increasing organic carbon sequestration, resulting in an accelerated restoration of ocean–atmosphere biogeochemistry during the termination phase of the PETM.

© 2017 Elsevier B.V. All rights reserved.

## 1. Introduction

One of the most abrupt and prominent decreases in δ<sup>13</sup>C throughout the Cenozoic has been documented ubiquitously in both terrestrial and marine geological records during the Paleocene–Eocene Thermal Maximum (PETM; ~56 Ma). A negative carbon isotope excursion of 2.5‰ or more (Kennett and Stott, 1991; McInerney and Wing, 2011) coincided with a global temperature increase of 5 to 8 °C (Zachos et al., 2003; Tripathi et al., 2009; McInerney and Wing, 2011), suggesting that the PETM was caused by an extraordinary input of isotopically light C into the ocean–atmosphere system. The massive (>3,000 Pg C) input of <sup>13</sup>C-depleted carbon during the onset of the PETM was injected into the system over at least 4,000 yr (e.g., Zachos et al., 2005; Zeebe et al., 2016). Although the exact source of the light car-

bon remains unknown, several potential mechanisms have been posited, including methane hydrate dissociation on the sea floor (Dickens et al., 1995, 1997; Zachos et al., 2005), terrestrial carbon sources (Kurtz et al., 2003; Pancost et al., 2007; DeConto et al., 2012) and oxidation of sedimentary organic carbon (Svensen et al., 2004). The entire event, including the onset, main phase and recovery, spanned a period of about 150,000–200,000 yr (Farley and Eltgroth, 2003; Murphy et al., 2010; Röhl et al., 2007), during which the excess carbon was ultimately removed from the ocean–atmosphere system through various biogeochemical feedbacks.

On long time scales, the primary restoring mechanism of excess carbon is via accelerated silicate weathering due to higher pCO<sub>2</sub>, temperature and an intensified hydrological cycle. However, the recovery of δ<sup>13</sup>C during the PETM was more rapid than anticipated for removal through enhanced silicate weathering alone (Dickens, 2001; Bowen and Zachos, 2010; Bowen, 2013). The rapid nature of the PETM recovery is often attributed to enhanced burial of organic matter (Bains et al., 2000; Dickens, 2001; Bowen and Zachos, 2010; Bowen, 2013) or explained by increased

\* Corresponding author.

E-mail address: komar@hawaii.edu (N. Komar).

net organic carbon storage (refueling of a putative organic carbon reservoir; e.g. methane hydrate capacitor) (Dickens, 2003). The biological production and removal of carbon from the surface ocean and its export and sequestration at the ocean bottom (biological carbon pump) might play an important role in regulating climate on multi-millennial time scales (Broecker, 1982), and it might have governed the pace and the duration of the PETM recovery. On long time scales, dissolved phosphorus (P) in the ocean is the nutrient that limits biological production (Tyrrell, 1999). The dissolved P concentration in the ocean depends on P inputs from the continents and burial in the sediments (Wallmann, 2010), as well as on the ambient redox conditions, which determine the rate of P burial/regeneration (Van Cappellen and Ingall, 1994; Slomp and Van Cappellen, 2007; Wallmann, 2003).

The riverine input of P is proportional to the silicate and carbonate weathering fluxes (Flögel et al., 2011). Hence, the elevated CO<sub>2</sub> and temperature during the PETM, and therefore globally enhanced continental weathering rates (Ravizza et al., 2001; Penman, 2016), should in theory entail greater primary production in the surface ocean through an increased nutrient supply from the continents. Data from various locations worldwide indicate that the nutrient supply was amplified during the PETM (e.g., Gibbs et al., 2006; Sluijs et al., 2006, 2009; John et al., 2008; Schulte et al., 2011). Consequently, increased marine paleo-production (Dickson et al., 2014) may have instigated a draw-down of bottom water oxygen. Indeed, there is evidence for reduced oxygen concentration during the PETM (e.g., Chun et al., 2010; Dickson et al., 2012; Pälike et al., 2014; Sluijs et al., 2014), which does not directly implicate enhanced production as the sole cause of the draw-down. Other mechanisms, such as oxidation of methane in the water column, might have been responsible. Regardless of mechanism, anoxic bottom waters may enhance P remineralization, leading to a higher dissolved P content of the surface ocean and therefore further increase in marine production and oxygen depletion (a positive feedback loop), while at the same time withdrawing more CO<sub>2</sub> from the atmosphere (Van Cappellen and Ingall, 1994). Furthermore, a lower O<sub>2</sub> concentration would lead to a greater organic carbon preservation and carbon burial. Therefore, increased CO<sub>2</sub> emissions during the PETM might have stimulated biological production, which would ultimately act as a mechanism for removing excess carbon from the ocean–atmosphere system. This hypothesis is consistent with the evidence of increased ocean primary production and carbon export during this time interval as inferred from marine barite accumulation rates (Bains et al., 2000; Ma et al., 2014) and coccolith Sr/Ca (Stoll and Bains, 2003).

Here, we utilize the LOSCAR (Long-term Ocean–atmosphere–Sediment Carbon cycle Reservoir) model to analyze the biogeochemical feedbacks between biological production, carbon (C), oxygen (O), phosphorus (P), and carbonate chemistry during massive CO<sub>2</sub> release events, such as the PETM. The original LOSCAR model was expanded to include a phosphorus cycle combining the works of Slomp and Van Cappellen (2007), Tsandev and Slomp (2009) and Flögel et al. (2011). The key objective is to investigate the role of a combined C–O–P feedback during the PETM and thus, provide a potential mechanism for the rapid removal of excess C from the ocean–atmosphere system consistent with the available PETM data and current understanding of the biogeochemical cycles involved. The PETM is dubbed the closest analogue for the ongoing anthropogenic climate change (Pagani et al., 2006; Zachos et al., 2008; Zeebe and Zachos, 2013). Therefore, quantifying the changes in phosphorus, biological production, oxygen concentration, and carbon removal as well as identifying the mechanisms initiating rapid carbon sequestration during the PETM may offer insight into future changes of biogeochemical processes in the ocean.

## 2. Model description

The model used in this study is an expanded version of the LOSCAR model (Zeebe, 2012). LOSCAR is comprehensively documented in Zeebe (2012) and has been used and tested in numerous earlier studies (e.g., Zeebe et al., 2008, 2009; Komar et al., 2013; Komar and Zeebe, 2016). Thus, aside from briefly covering the major features of LOSCAR (below), we abstain from explaining the model in greater detail here. However, the expansion of the model pertaining to the P cycle will be thoroughly discussed.

LOSCAR is a 13-box (paleo-version) ocean model with an additional box representing the atmosphere, coupled to a sediment model. It efficiently computes the partitioning of carbon between ocean, atmosphere and sediments on a wide range of time scales, from centuries to millions of years. The volumes of ocean boxes are based on realistic Paleocene/Eocene ocean basin topography (Bice et al., 1998). The model includes a variety of biogeochemical tracers such as total carbon (TC), total alkalinity (TA), phosphate, oxygen, calcium and stable carbon and calcium isotopes. Using the model predicted evolution of TC and TA values, numerous seawater carbonate parameters ([CO<sub>2</sub>], [CO<sub>3</sub><sup>2-</sup>], pH, calcite and aragonite saturation state) are computed using algorithms explained in Zeebe and Wolf-Gladrow (2001). Weathering of carbonate and silicate rocks is parameterized as a function of atmospheric CO<sub>2</sub> (Uchikawa and Zeebe, 2008; Zeebe, 2012).

The main components of the reactive phosphorus cycle include river input ( $F_{PW}$ ), primary production, remineralization and sediment burial. The latter involves burial of particulate organic P (POP; associated with living and detritus marine biomass), which is comprised of organic material that rains down from the surface ocean, escapes remineralization, and reaches the sediments where it is buried ( $F_{OPB}$ ). Phosphorus is also buried in the sediments associated with authigenic ferric iron oxides ( $F_{FeP}$ ) or precipitated as authigenic carbonate fluorapatite ( $F_{CaP}$ ) (Slomp and Van Cappellen, 2007) (see Table 1). There is no explicit diagenetic sediment model associated with the P burial and the LOSCAR P cycle version (LOSCAR-P for short) does not account for biogenic P burial fluxes from fish debris. Therefore, in addition to the original internal LOSCAR phosphate fluxes (Zeebe, 2012), the change of the phosphate concentration ([PO<sub>4</sub>]) is governed by four additional external terms as described above:

$$\left. \frac{d[\text{PO}_4]}{dt} \right|_{ex} = F_{PW} - (F_{OPB} + F_{CaP} + F_{FeP}). \quad (1)$$

In LOSCAR, primary production rates are parameterized based on the phosphate concentration in the ocean surface layer. The biological uptake fluxes of PO<sub>4</sub> are related to the primary production via the Redfield-ratio (C/P = 130) (Takahashi et al., 1985). The total initial export production from the surface ocean, controlled by [PO<sub>4</sub>] and the biopump efficiency ( $f_{ep} = 80\%$ ), Zeebe (2012) is around 460 Tmol C/yr, which is almost identical to the value estimated for the pre-PETM period (Ma et al., 2014; value estimated from barite accumulation rates using a modern relationship). In the default LOSCAR-P set-up (control run), a large fraction (99%) of the carbon export flux ( $F_{Cexp}$ ) is remineralized in the intermediate and deep ocean boxes, while the remainder (fraction of organic carbon buried ( $f_{OC}$ ); initially set to 1%) is lost to the sediments. On the other hand, the C/P ratio in buried organic matter depends on the redox state of bottom waters (Van Cappellen and Ingall, 1994; Tsandev and Slomp, 2009) and is initially about twice as large (~250) as the ratio in the surface water (see below). In order to achieve this C/P in buried organic matter in LOSCAR-P, the fraction of the export flux of P ( $f_{OP}$ ) from the surface ocean buried in sediments was set to half (0.5%) the fraction of organic C export ( $f_{OC} = 1\%$ ) buried in sediments. Therefore, the organic C burial flux

**Table 1**

Steady-state fluxes for the standard model run.

| Fluxes:    |                                   |   |   |
|------------|-----------------------------------|---|---|
| $F_{Cexp}$ | Carbon export flux                | $4.6 \times 10^2 \text{ Tmol yr}^{-1}$    |   |
| $F_{Pexp}$ | Biological fixation of reactive P | $3.52 \text{ Tmol yr}^{-1}$               | $\frac{F_{Cexp}}{130}$                      |
| $F_{OCB}$  | Org. C burial                     | $4.6 \text{ Tmol yr}^{-1}$                | 1% of $F_{Cexp}$                            |
| $F_{OPB}$  | Org. P burial                     | $1.76 \times 10^{10} \text{ mol yr}^{-1}$ | $\frac{F_{OCB}}{260} = 0.5\%$ of $F_{Pexp}$ |
| $F_{CaP}$  | CaP burial                        | $3.52 \times 10^{10} \text{ mol yr}^{-1}$ | 50% of total POP                            |
| $F_{FeP}$  | FeP burial                        | $1.76 \times 10^{10} \text{ mol yr}^{-1}$ | 25% of total POP burial                     |
| $F_{OCW}$  | Kerogen oxidation                 | $4.6 \text{ Tmol yr}^{-1}$                | for steady-state                            |
| $F_{PW}$   | Phosphate weathering flux         | $7.04 \times 10^{10} \text{ mol yr}^{-1}$ | for steady-state                            |

is initially 260 times larger than the organic P burial flux (Table 1); 130 times larger at the surface due to Redfield and additional two times larger due to the burial ratios (see  $f_{OC}$  and  $f_{OP}$  fractions).

Nitrate (N) in LOSCAR is parameterized based on the C to N Redfield-ratio (C/N = 130/15). Uptake and release of nitrate contributes to alkalinity changes in the model. In LOSCAR-P, the changes in alkalinity due to changes in the above mentioned P fluxes (and hence N) also need to be accounted for. The original LOSCAR version (without the P burial cycle) assumes that the export from the surface ocean of the elements P and N is completely remineralized in the intermediate and deep boxes. In LOSCAR-P, a portion of the export flux is buried in the sediments and therefore not remineralized (in order to balance the riverine input flux). Due to the Redfield ratio link between N and P, nitrate taken up from the surface that reaches the deep ocean is also not fully respired, which creates an alkalinity imbalance. The nitrate and phosphate portion of the export flux that is not respired (remineralized) represents an alkalinity source (Wolf-Gladrow et al., 2007). This additional source of alkalinity is balanced by the riverine input of nitrate and phosphate which acts as an alkalinity sink.

Unlike the P model of Tsandev and Slomp (2009), Slomp and Van Cappellen (2007), and Flögel et al. (2011), LOSCAR-P does not include a separate representation of the shelf and deep oceans. In other words, the entire P that is buried is removed from the deep boxes. The burial of P (and C), which is redox dependent, is therefore based on the mean deep ocean oxygen concentration (Lenton and Watson, 2000).

### 2.1. Redox-controlled reactive P and organic C burial

The organic phosphate burial flux ( $F_{OPB}$ ) is assumed to be proportional to the export flux ( $F_{Pexp}$ ) from the surface ocean (Tsandev and Slomp, 2009):

$$F_{OPB} = f_{OP} \times F_{Pexp} \times \left( 0.25 + 0.75 \frac{[O_2]}{[O_2]_0} \right), \quad (2)$$

where  $f_{OP}$  is the fraction of the export flux that is buried in the sediments, initially set to 0.5%. This flux is also dependent on water column oxygenation (Slomp and Van Cappellen, 2007; Tsandev and Slomp, 2009).  $[O_2]_0$  is the bottom water oxygen concentration at time  $t = 0$ , which corresponds to modern deep ocean oxygen concentration (Slomp and Van Cappellen, 2007). However, in our model  $[O_2]_0$  represents the pre-PETM steady-state concentration. Burial of organic P is reduced by up to 75% under full anoxia, while the burial of organic carbon increases (Eq. (3); Slomp and Van Cappellen, 2007; Tsandev and Slomp, 2009).

The  $F_{OPB}$  and  $F_{OCB}$  fluxes are coupled through the organic matter C to P burial ratio, which is significantly larger than the Redfield value (Slomp and Van Cappellen, 2007; Tsandev and Slomp, 2009, and references therein). This ratio also depends on the redox-state of the bottom waters (Tsandev and Slomp, 2009):

$$\frac{F_{OCB}}{F_{OPB}} = \frac{\left( \frac{C}{P} \right)_{oxic} \times \left( \frac{C}{P} \right)_{anoxic}}{\frac{[O_2]}{[O_2]_0} \times \left( \frac{C}{P} \right)_{anoxic} + \left( 1 - \frac{[O_2]}{[O_2]_0} \right) \times \left( \frac{C}{P} \right)_{oxic}}, \quad (3)$$

where  $\left( \frac{C}{P} \right)_{oxic} = 260$  and  $\left( \frac{C}{P} \right)_{anoxic} = 4000$  (Ingall et al., 1993), represent end-member values for organic matter buried under completely oxic and fully anoxic deep water conditions, respectively.

The P flux associated with ferric iron oxides is linearly correlated to changes in oxygen concentration of the deep water (Tsandev and Slomp, 2009):

$$F_{FeP} = F_{FeP}^0 \times \frac{[O_2]}{[O_2]_0}, \quad (4)$$

where  $F_{FeP}^0$  is  $F_{FeP}$  at time  $t = 0$  (pre-PETM steady-state rate).

Precipitation of authigenic CaP is formulated as follows (Tsandev and Slomp, 2009):

$$F_{CaP} = f_{CaP} \times POP_{remin} \times \left( 0.1 + 0.9 \frac{[O_2]}{[O_2]_0} \right) \quad (5)$$

where  $f_{CaP}$  is a fraction of reactive P that is produced by decomposition of organic matter and is converted into CaP. Its value is 0.005 and is set to satisfy the steady-state condition.  $POP_{remin}$  is remineralization flux of P, which is equal to the difference between export and burial. Thus:

$$POP_{remin} = F_{Pexp} \times (1 - f_{OP}). \quad (6)$$

The phosphorus weathering flux is assumed to be regulated by the rates of chemical weathering and should therefore scale with the change in cumulative carbonate and silicate weathering rates (Flögel et al., 2011):

$$F_{PW} = F_{PW}^0 \times \frac{F_{WC} + F_{Si}}{F_{WC0} + F_{Si0}}, \quad (7)$$

where  $F_{PW}^0$ ,  $F_{WC0}$ , and  $F_{Si0}$  are riverine input of dissolved phosphorus, carbonate, and silicate weathering at time  $t = 0$  (pre-PETM steady-state rate), respectively.

### 3. PETM simulations

The carbon perturbation used in this study involves a C input of 3,000 Pg C ( $\delta^{13}C = -50\text{‰}$ ) in the form of methane to the deep Atlantic and/or atmosphere over 5,000 yr. For simplicity and easier quantification of biogeochemical effects and mechanisms, an additional continuous release of carbon (referred to as “leak”), described as the preferred PETM scenario (Zeebe et al., 2009), in the amount of 1480 Pg C over ~40 kyr was initially omitted (Figs. 1–4). For the same reason, the prescribed circulation change in the original LOSCAR simulation (Zeebe et al., 2009) was also turned off. However, the leak feature in combination with new P burial model will be included later (Fig. 5) to model the PETM more realistically and in order to constrain the amount of carbon drawdown during the PETM recovery phase.

We first perturb the ocean–atmosphere system and compare the responses of different LOSCAR versions in order to demonstrate the effect of the newly introduced P burial cycle. The three different versions of LOSCAR are color-coded so that colors are consistent between panels (Fig. 1). Time  $t = 0$  corresponds to the onset

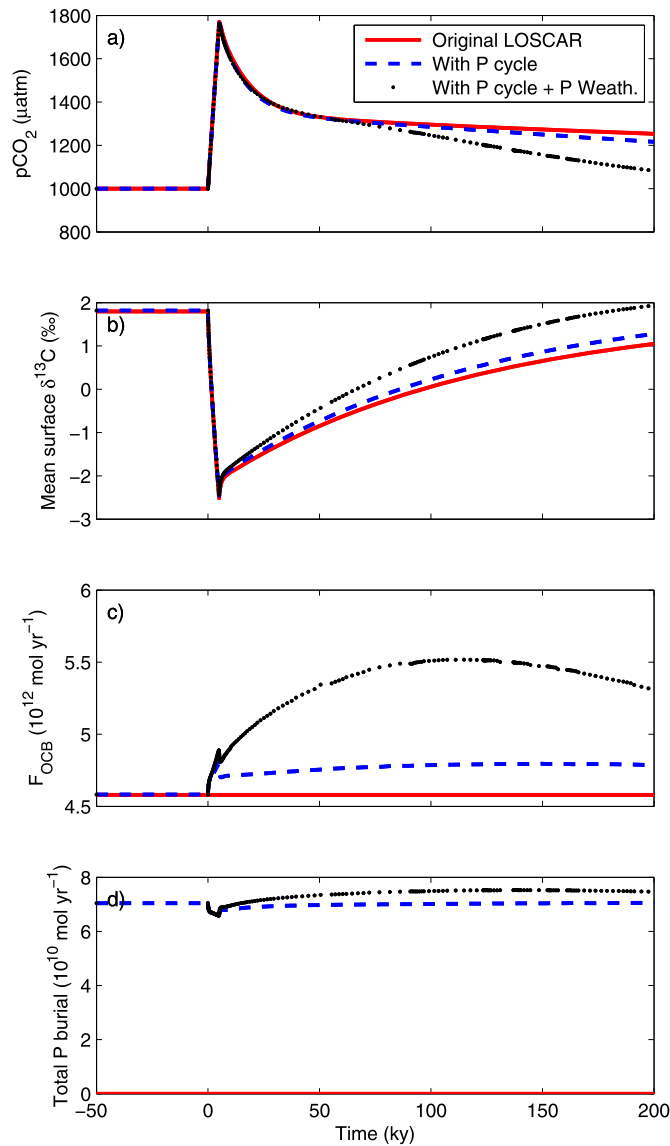


**Fig. 1.** Comparison of responses of different LOSCAR model versions to a 3000 Pg C perturbation. a) Atmospheric  $\text{CO}_2$  b) Mean surface  $\delta^{13}\text{C}$  c) Organic carbon burial flux d) Total P burial flux ( $F_{\text{CaP}} + F_{\text{OPB}} + F_{\text{FeP}}$ ). Solid red line: the original LOSCAR model without P burial. Dashed blue line: LOSCAR-P burial but with constant P riverine input. Dotted black line: LOSCAR-P burial and  $\text{CO}_2$  dependent P weathering (LOSCAR-P control run). The results displayed in red, blue and black lines correspond to LOSCAR without P burial cycle, LOSCAR that includes P burial cycle but P weathering is constant, and LOSCAR version with P cycle in which P weathering is  $\text{pCO}_2$ -dependent (LOSCAR-P), respectively. The black line represents the LOSCAR-P control run, with steady-state fluxes outlined in Table 1. (For interpretation of the references to color in this figure legend, the reader is referred to the web version of this article.)

of the PETM (Paleocene–Eocene boundary), when the simulation is initiated by perturbing the system with the input of light carbon. Because the original LOSCAR version (red lines, Fig. 1) does not include a P burial cycle and there is no redox feedback between P and C, both P and organic C burial fluxes remain constant over time (Fig. 1c and 1d). On the other hand, LOSCAR-P accounts for the redox dependency and thus displays a variable trend in P and C burial. It is apparent that the LOSCAR-P version exhibits a more rapid  $\text{pCO}_2$  drop as well as a faster  $\delta^{13}\text{C}$  recovery. This is due to an increase in organic carbon burial as a consequence of both increased  $[\text{PO}_4]$  (and consequently larger carbon export flux; Fig. 2) and a decrease in oxygen concentration (Fig. 3a). The amount of excess carbon buried in the control LOSCAR-P simulation due to

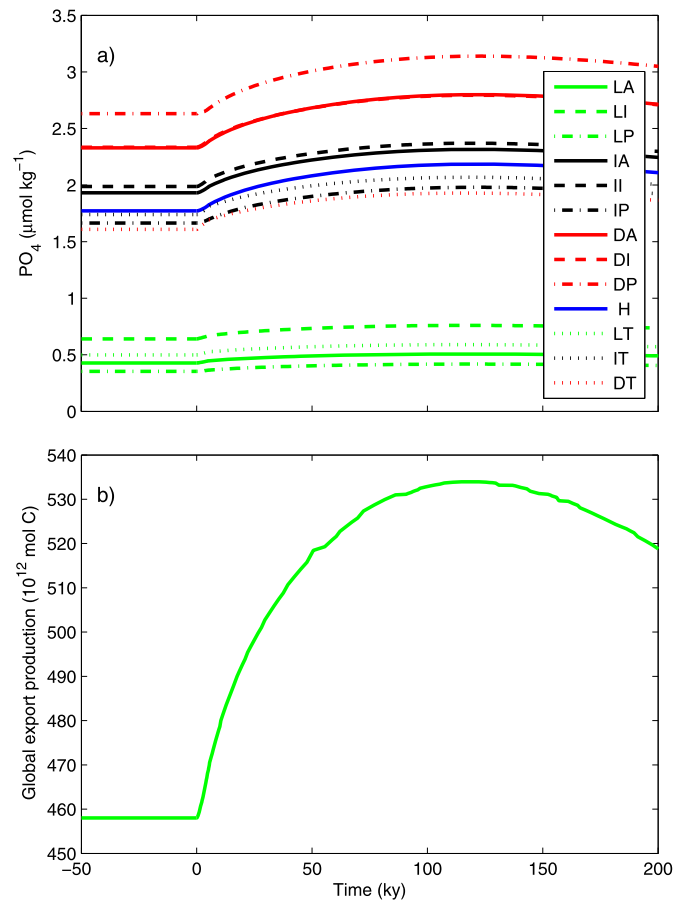


**Fig. 2.** Oceanic phosphate concentration (a) and global export production (b) in response to a 3000 Pg C perturbation in the control LOSCAR-P run. L, I, and D correspond to surface, intermediate, and deep ocean boxes, respectively. A, I, P, and T represent Atlantic, Indian, Pacific, and Tethys ocean, respectively. (For interpretation of the colors in this figure, the reader is referred to the web version of this article.)

the C–O–P feedback (black line, Fig. 1) over the entire 200 ky period is  $\sim 1800$  Pg C. The details of the feedback are discussed in section 4.

The response of the phosphate concentration to the carbon perturbation in different ocean boxes (Fig. 2a) in the LOSCAR-P control run is a combination of increased weathering fluxes as well as changes in P burial fluxes due to variable deep ocean oxygen concentration (Fig. 3a). All ocean boxes display an increase in  $[\text{PO}_4]$ , which in turn affects the amount of carbon export from the surface ocean (Fig. 2b). The initial burial fluxes,  $F_{\text{CaP}}$ ,  $F_{\text{OPB}}$ ,  $F_{\text{FeP}}$  are set in proportion of 50%, 25%, 25% of total reactive P burial based on preindustrial conditions (Ruttenberg, 1993) (Fig. 3b). Initially, the  $F_{\text{OPB}}$  is set as a fraction (which we vary in sensitivity experiments, see below) of the export from the surface (Eq. (2)). Using the proportion stated, the other two P burial fluxes ( $F_{\text{CaP}}$  and  $F_{\text{FeP}}$ ) are calculated. Therefore in order to achieve a steady-state, the riverine input of P is set to match the total P burial flux. The total inventory of dissolved  $\text{PO}_4$  in the ocean in the control run is  $\sim 3 \times 10^{15}$  mol P and the total burial flux is  $\sim 7 \times 10^{10}$  mol  $\text{yr}^{-1}$ , hence the residence time of P in the ocean is  $\sim 43,000$  yr.

The main controls on oceanic oxygen concentration in the model are seawater temperature, productivity and nutrient cycling, as well as oxidation of reduced carbon (Fig. 3a). The combined effect of these processes results in a general oxygen decrease over time in all ocean boxes (Fig. 3a). The sudden and more pronounced drop in  $[\text{O}_2]$  in the deep Atlantic ocean is due to the oxidation of methane injected into this model box. The control run assumes that 40% of carbon is oxidized in the deep Atlantic, Deep Atlantic

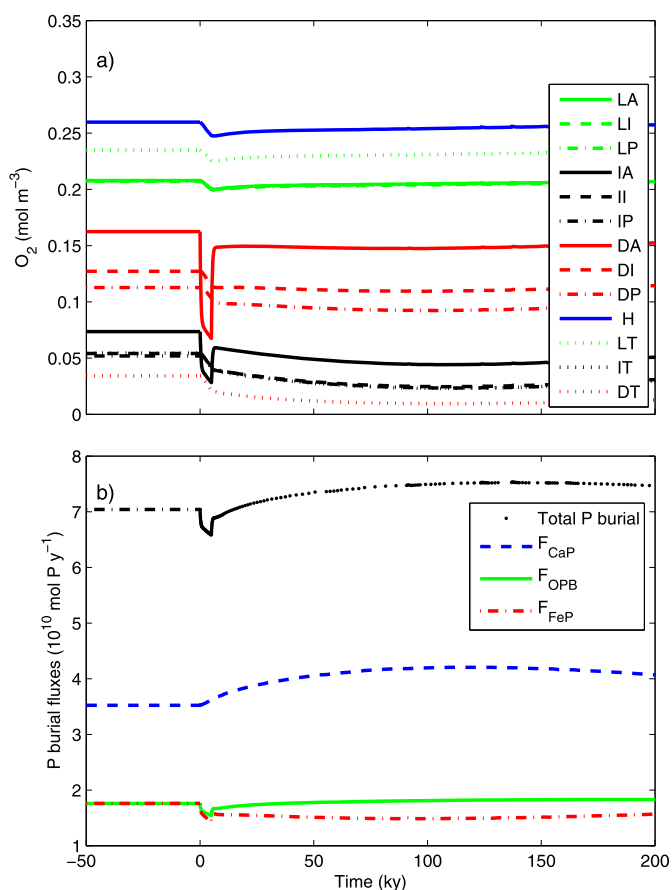


**Fig. 3.** Evolution of the dissolved oxygen concentration (a) and phosphorus burial fluxes (b) to a 3000 Pg C perturbation in the control LOSCAR-P run. (For interpretation of the colors in this figure, the reader is referred to the web version of this article.)

Oxidation (DAO) in the following (Zeebe et al., 2009). Sensitivity experiments revealed that the DAO fraction has a negligible effect on overall excess carbon burial and carbon isotope recovery during the PETM (see Supplement). We also explored the model sensitivity to a wide range of global P weathering and burial fluxes as well as kerogen oxidation and carbon burial. Since we assumed that the light carbon was injected in methane form (potentially from an organic carbon capacitor such as methane hydrates), an additional scenario is considered. This scenario takes into account the change in net organic C flux of the aforementioned capacitor (capacitor recharge) that would arise during the recovery phase of the PETM. Due to length constraints, the model runs outlined above are presented in the Supplement but a brief synopsis of the results is presented in Section 4.1.

Next, we include the additional carbon leak of 1,480 Pg C over 42,000 yr (Zeebe et al., 2009), mentioned above, to investigate the main and recovery phase of the PETM and compare the results of the original LOSCAR and LOSCAR-P models (Fig. 5). For LOSCAR-P, we also added a scenario with a stronger leak (2,500 Pg C between 20 and 62 ky after the onset; our preferred scenario, see below) in order to get a prolonged carbon isotope excursion (Fig. 5, green line) during the PETM main phase, which is more consistent with the  $\delta^{13}\text{C}$  data (Fig. S4). The initial P and C burial fluxes in the strong-leak scenario (leak = 2,500 Pg C) are identical to those used in the standard leak scenario (leak = 1,480 Pg C;  $f_{OP} = 1.00\%$  and  $f_{OC} = 2.00\%$ ; Fig. 5, red line). In the original LOSCAR model, the organic carbon burial remains constant, for the reasons explained earlier. The calculated excess C burial, using the same set of conditions as in the control LOSCAR-P run but with the leak included, is

$\sim 2,500$  Pg C (Fig. 5, dashed black line). Doubling the initial carbon and phosphorus burial rates results in an overall excess C burial of about 4,300 Pg C. The excess C burial during the entire PETM period in the “stronger-leak” scenario is  $\sim 5,400$  Pg C.

Out of the four scenarios outlined above, the “stronger-leak” scenario, combined with enhanced initial carbon and phosphorus burial rates produces the swiftest  $\delta^{13}\text{C}$  recovery (Fig. 5c). Depending on the age model used, the recovery phase of the PETM appears to have lasted between 30,000–40,000 yr ( $^3\text{He}$  age model; Farley and Eltgroth, 2003; Bowen and Zachos, 2010) or in the excess of 100 ky (cyclostratigraphic age model; Röhl et al., 2007) (see Supplement). In our model, the recovery starts at around 60 ky after the onset, when the system is no longer perturbed by the input of light carbon. The integrated excess C burial between 60 ky and 100 ky (recovery phase duration according to the  $^3\text{He}$  model) in our model in the strong leak scenario is 1,700 Pg C, which is close to the proposed amount of 2000 Pg C needed to explain the observed  $\delta^{13}\text{C}$  recovery rate (Bowen and Zachos, 2010).

Additionally, we compare the responses of the calcite compensation depth (CCD) as well as  $\text{CaCO}_3$  wt% at two different depths for different “leak” scenarios described above (Fig. 6). The simulation of the CCD evolution can be used as an additional model benchmark by reproducing the CCD trends that are consistent with observations. Particularly, examining whether a certain scenario produces an over-deepening (overshoot) of the CCD during the PETM recovery phase, which is evident in many sediment sections (Zachos et al., 2005; Leon-Rodriguez and Dickens, 2010; Kelly et al., 2005; Slotnick et al., 2015; Penman et al., 2016). The most notable difference in the CCD response between the original LOSCAR (Fig. 6, solid blue line) and LOSCAR-P during the recovery stage is that the CCD overshoot in the LOSCAR-P model is muted or not present at all (Fig. 6, dashed black line). The mechanism responsible for the reduced CCD deepening during the recovery stage and implications of the result are discussed in more detail in Section 4.3.

## 4. Discussion

### 4.1. The feedback between carbon, oxygen and phosphorus

Our results imply that the feedback between carbon, oxygen, and phosphorus cycling in the ocean-atmosphere system may ultimately lead to enhanced organic carbon sequestration during large carbon emission events. The feedback mechanism is set in motion once the system is perturbed with a large enough quantity of carbon, which triggers a series of events, starting with an increase in atmospheric  $\text{CO}_2$  (Fig. 1a) and global warming. Warmer temperatures lead to an intensified hydrological cycle and accelerated weathering of phosphate minerals, eventually resulting in higher phosphate concentration in the sea (Fig. 2a). Being the limiting nutrient, higher phosphorus content in the surface ocean instigates a stronger biological production and larger carbon export to the deep ocean (Fig. 2b), which is consistent with paleo-export production data derived from marine barite accumulation rates for the PETM (Bains et al., 2000; Ma et al., 2014) and coccolith Sr/Ca (Stoll and Bains, 2003).

Concurrent with the phosphate content increase is a decline in oxygen concentration (Fig. 3a). There are two different processes in the model that both contribute to the oxygen draw-down. First, the rising global temperature reduces the amount of dissolved oxygen in the water column by lowering the solubility of oxygen (Weiss, 1970), thus we observe a long-term oxygen drop in all ocean basins (Fig. 3a). Second, due to a carbon input in the deep Atlantic, the simulated oxygen concentration in this basin plunges temporarily as a result of carbon input and its subsequent oxidation. This model behavior is in line with many previous studies that

indicate a reduction in oxygenation of seawater during the PETM (e.g., Chun et al., 2010; Dickson et al., 2012; Pälike et al., 2014; Sluijs et al., 2014).

The dependence of C and P burial on the redox state of the ocean is described mathematically in Section 2.1 (Eqs. (2)–(6)). Lowered oxygen concentration diminishes the organic carbon remineralization rate and therefore results in a higher organic carbon preservation and burial (e.g., Hartnett et al., 1998). At the same time, lowered oxygen content allows for enhanced P regeneration (e.g. Ingall et al., 1993) and the eventual refueling of the surface ocean with more nutrients, which then amplifies the primary production and carbon export and preservation, thus accelerating  $\text{CO}_2$  and  $\delta^{13}\text{C}$  recovery even further in a positive feedback loop. It is worth mentioning that the warming ( $\sim 3.5^\circ\text{C}$  at most) predicted by LOSCAR (using the canonical climate sensitivity of 3 K per  $\text{CO}_2$  doubling) through the radiative forcing of the  $\text{CO}_2$  underestimates the warming reconstructed from proxies ( $>5^\circ\text{C}$ ) (Zeebe et al., 2009). Therefore the long-term  $\text{O}_2$  decline caused by the solubility decrease would have been even more pronounced in reality, which would have resulted in a higher excess organic C burial through the redox dependence.

The variations in phosphorus burial fluxes are primarily driven by the redox feedbacks and/or the export production from the surface ocean. Burial of phosphorus bound to iron oxides (Fig. 3b, dotted-dashed red line) has a direct linear relationship to the mean oxygen concentration of the deep ocean (Eq. (4)) and thus follows a similar trend to that of oxygen. Therefore, less P is buried (more regenerated) through  $F_{FeP}$  as oxygen concentration decreases and in theory, no P could be buried at all in completely anoxic waters (Tsandev and Slomp, 2009). The burial flux of the organic phosphorus (Fig. 3b, solid green line), unlike  $F_{FeP}$ , not only depends on the oxygenation but also on the export production from the surface ocean. As the  $\text{O}_2$  concentration plummets over the first several thousand years, due to methane oxidation, so does the organic phosphorus burial. However, as the export production increases due to rising surface ocean  $[\text{PO}_4]$  (Fig. 2), the organic P burial starts to recover, eventually reaching rates slightly higher than the initial, even though the oxygen concentration remains below the initial levels. The removal of P via authigenic  $F_{CaP}$  exhibits a different behavior from the other two previously described P burial fluxes by staying elevated for the entire duration of the run (Fig. 3b, dashed blue line). Although  $F_{CaP}$  is also redox dependent (Eq. (5)) and thus expected to decrease during the water deoxygenation, the burial rate remains above the initial value even during the strongest oxygen depletion that takes place throughout the first several thousand years of the simulation. This is due to the fact that  $F_{CaP}$  also depends on P regeneration, which is the difference between the export and burial rate of phosphorus (Eqs. (5) and (6)). As the burial rate of P is attenuated in the first several thousand of years while the export simultaneously increases, the regeneration rate is intensified and overpowers the reduction in  $F_{CaP}$  that results from a decrease in oxygen concentration. The total P burial is simply the sum of all three P burial fluxes accounted for in the model (Fig. 3b, dotted black line).

Organic carbon burial and P burial in the deep ocean are linked through the C to P burial ratio of the buried organic matter (Eq. (3)). Eq. (3) accounts for the effect of oxygen on the C to P ratio based on observations, which suggests ratios considerably higher than Redfield, especially under anoxic conditions (e.g., Ingall et al., 1993; Filippelli, 2001). Thus, according to the equation, organic C burial is directly proportional to organic P burial and inversely related to oxygen concentration. Therefore, as the deep ocean oxygen concentration drops, the rate of carbon burial increases, as shown across all of our LOSCAR-P simulations (e.g. Fig. 1c). The amount of cumulative excess carbon burial during the entire duration of the PETM is sensitive to the initial C burial/kero-

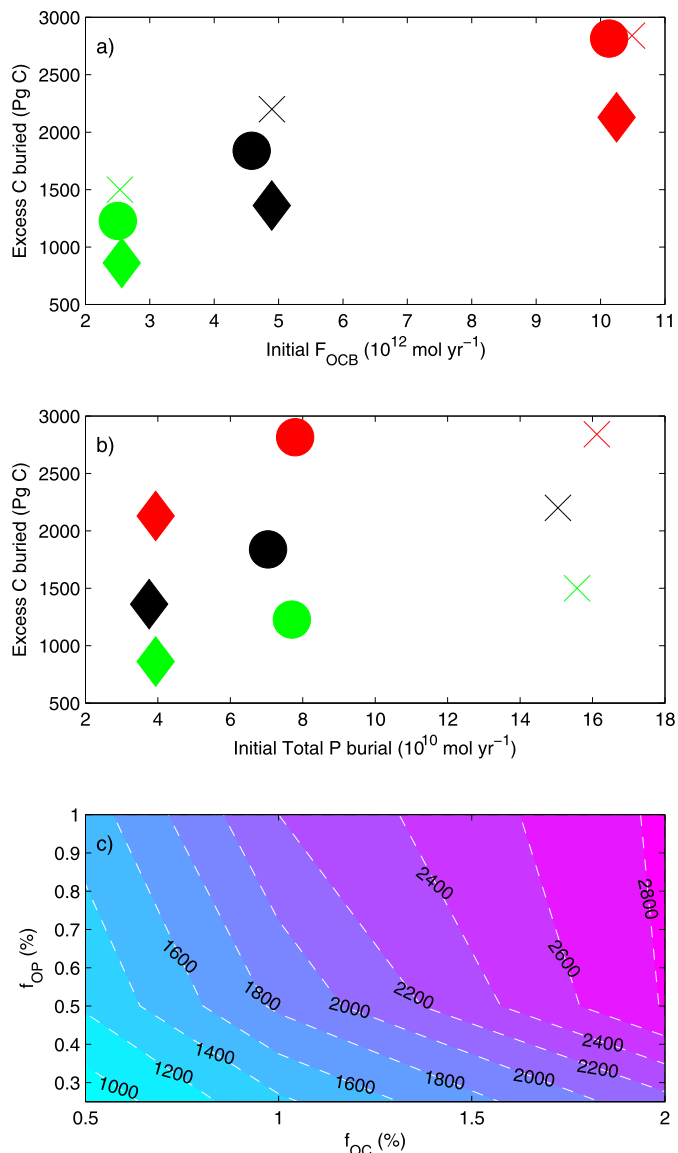


**Fig. 4.** Summary of LOSCAR-P sensitivity experiments to the initial fraction of organic phosphorus ( $f_{OP}$ ) and organic carbon buried ( $f_{OC}$ ) in the deep ocean shown in the Supplement (Fig. S2). a) Excess carbon burial over 200 ky as a function of the initial organic carbon burial flux b) Excess carbon burial over 200 ky as a function of the initial organic phosphorus burial flux c) The combined effect of  $f_{OC}$  and  $f_{OP}$  on excess carbon burial over 200 ky. The same color coding for  $f_{OC}$  is applied as in Fig. S2: diamonds, circles and crosses correspond to  $f_{OP} = 0.25, 0.50,$  and  $1.00\%$ , respectively; green, black, and red colors correspond to  $f_{OC} = 0.50, 1.00,$  and  $2.00\%$ , respectively. (For interpretation of the references to color in this figure legend, the reader is referred to the web version of this article.)

gen oxidation flux and P burial/riverine flux (Figs. 4 and S2) but the relationship is not linear. For example, quadrupling both the initial P and C fluxes increases the overall excess C burial by a factor of 3.3. The modeled overall excess C burial is less sensitive to the initial P burial than C burial (Fig. 4), however it is important since it directly affects the residence time of P in the ocean. With higher throughput of P, and therefore shorter residence time of phosphorus in the ocean, the peak P burial fluxes, and consequently C burial fluxes, are achieved much earlier when compared to simulations with initially lower P burial (Fig. S2c and S2d). The rates also recover faster in simulations with high initial P burial (compare red lines in Fig. S2c), so the excess accumulation period of C is shortened, producing less C burial over the last 75 ky compared to the low initial P simulations. This is the reason for the

non-linearity and for a decrease in C sequestration sensitivity at higher initial P burial rates (Fig. 4).

#### 4.2. Organic carbon burial and $\delta^{13}\text{C}$ in the sediment record

Data from certain paleo-locations support the idea that the PETM might have gone through a phase of elevated organic carbon burial, compared to the pre-PETM conditions (John et al., 2008; Sluijs et al., 2006), which is a behavior predicted by our model. Using the present day continental shelf area, John et al. (2008) extrapolated the excess cumulative mass accumulation rates data of organic carbon from the North American continental margin to provide a very crude estimate of the global excess cumulative carbon burial during the PETM. Their estimates shows that about 2200 to 2900 Pg C could have been sequestered, this number is even larger if the actual Eocene continental shelf area is used, considering a higher sea level. They show that organic carbon mass accumulation rates remained elevated throughout the entire duration of the PETM. Furthermore, the peak excess accumulation lags the peak in carbon isotope excursion and it stays intensified even during the PETM recovery phase, similar to the shape of organic C burial predicted by LOSCAR-P (Fig. 7).

It has been suggested that a transient increase in organic burial during the recovery stage of the PETM is necessary in order to produce the rapid CIE recovery observed in the record (Bowen and Zachos, 2010). Bowen and Zachos (2010) explain the rapid recovery by assuming an ad-hoc increase in organic carbon burial without providing a process-based mechanism for accelerated carbon storage. Our model indicates that significant sequestration of organic carbon can arise due to the C–O–P feedback, without employing any ad-hoc, temporary increases in carbon removal (Fig. 5d, green line; 1,700 Pg C stored during the recovery stage). During the PETM main phase (between  $\sim 20$  ky and 60 ky)  $\delta^{13}\text{C}$  is in quasi-steady-state, since the external input of light carbon is temporarily in balance with its removal via carbon burial and thus the  $\delta^{13}\text{C}$  remains close to constant (Fig. 5c, green line). The leak of light carbon ceases after  $\sim 60$  ky, while the organic C burial rate is at its highest at this point due to the C–O–P feedback explained above. Hence,  $\delta^{13}\text{C}$  starts to recover rapidly, owing to a massive draw-down of light carbon that comes from accelerated organic carbon burial, until a new steady-state is achieved. The general trend and behavior of the modeled  $\delta^{13}\text{C}$  is consistent with observations but the amount of carbon sequestered during the PETM recovery-phase (1,700 Pg C) is slightly smaller than that calculated by Bowen and Zachos (2010) (2,000 Pg C, which might be an upper limit). However, the value they calculated depends heavily on the age model and the location of  $\delta^{13}\text{C}$  data used. This is problematic because of large inconsistencies associated with the actual data and age models (see Supplement).

#### 4.3. The CCD and $\text{CaCO}_3$ content

Simulation of adequate CCD changes during the PETM may serve as an additional model constraint (Zeebe et al., 2009; Penman et al., 2016). In carbon cycle models accounting for the feedback between atmospheric  $\text{CO}_2$  and carbonate and silicate weathering, the CCD exhibits a behavior in which its position deepens during the recovery stages of the PETM compared to prior to the event (e.g., Zeebe et al., 2009; Zeebe and Zachos, 2013). The CCD over-deepening is caused by the  $\text{pCO}_2$ -weathering feedback. The carbon input during the PETM main phase raises the atmospheric  $\text{pCO}_2$  which remains elevated even after the carbon input has stopped (Fig. 5a–5b), temporarily diminishing the carbonate saturation state of the ocean and reducing the burial of  $\text{CaCO}_3$ . Simultaneously, the elevated atmospheric  $\text{CO}_2$  (and accompanying changes in temperature, hydrological cycle, plant productivity, pH

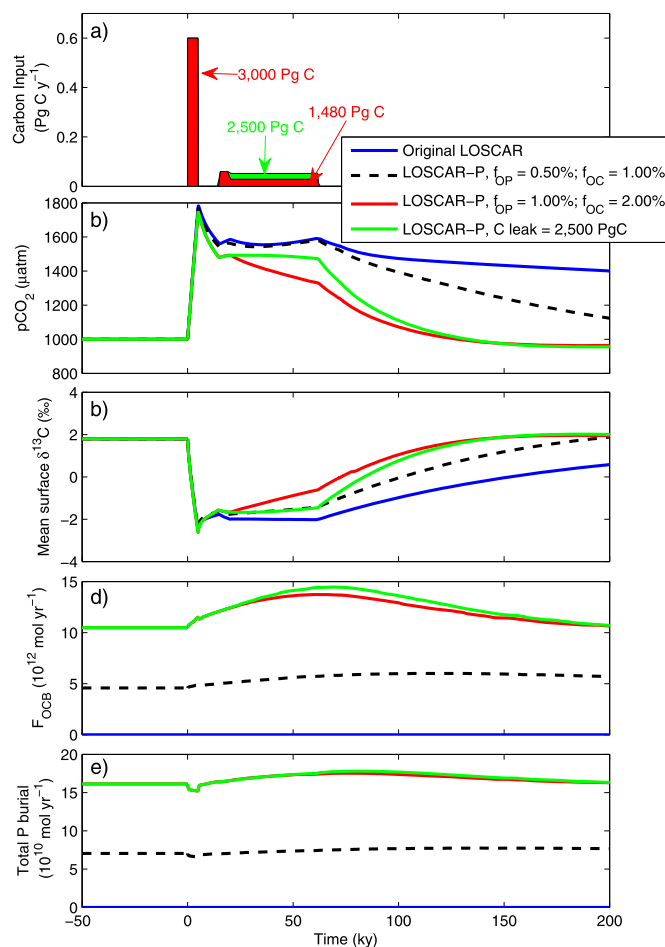


**Fig. 5.** Comparison of responses of original LOSCAR and LOSCAR-P to the PETM scenario including the “leak” of carbon over 42,000 yr during the main phase. a) Carbon release scenarios: Every simulation shown here has a main emission of 3000 Pg C over 5 ky, followed by an additional leak of 1,480 Pg C, except for the “strong leak” simulation (denoted in green), which has a leak of 2,500 Pg C. b) Atmospheric  $\text{CO}_2$  c) Mean surface  $\delta^{13}\text{C}$  d) Organic carbon burial flux e) Total reactive P flux ( $F_{\text{CaP}} + F_{\text{OPB}} + F_{\text{FeP}}$ ). (For interpretation of the references to color in this figure legend, the reader is referred to the web version of this article.)

of the soil etc.) accelerates the weathering of carbonate and silicate rocks, resulting in enhanced input of calcium and carbonate ions to the ocean. The imbalance between the inputs and outputs during the recovery stage of the PETM creates a surplus of  $\text{Ca}^{2+}$  and  $\text{CO}_3^{2-}$ , raising the saturation state of the ocean. The saturation state of the ocean continues to rise until a temporary steady-state between the influx and burial is established. This quasi-steady state of carbonate saturation is higher than initially, because it is maintained at higher  $\text{pCO}_2$  levels, and therefore the CCD is deepened in order to accommodate a larger carbonate burial rate needed to balance an enhanced input from weathering (see section 4.4).

Indirect lines of evidence support the model prediction and suggest that the carbonate preservation during the PETM recovery was noticeably higher than prior to the event (e.g., Kelly et al., 2010), implying a suppressed CCD. Until recently, however, there was no direct evidence of a transient CCD over-deepening during the recovery stage of the PETM because all sediment sections recovered from this time period were positioned above the CCD. The carbonate content data recently presented in Penman et al. (2016) provide the first validation for the CCD overshoot, which appears in the record 70 ky after the onset of the PETM (based on a cyclostratigraphic age model) at IODP sites U1403 and U1409 in the North Atlantic. This CCD overshoot feature along with a slight in-

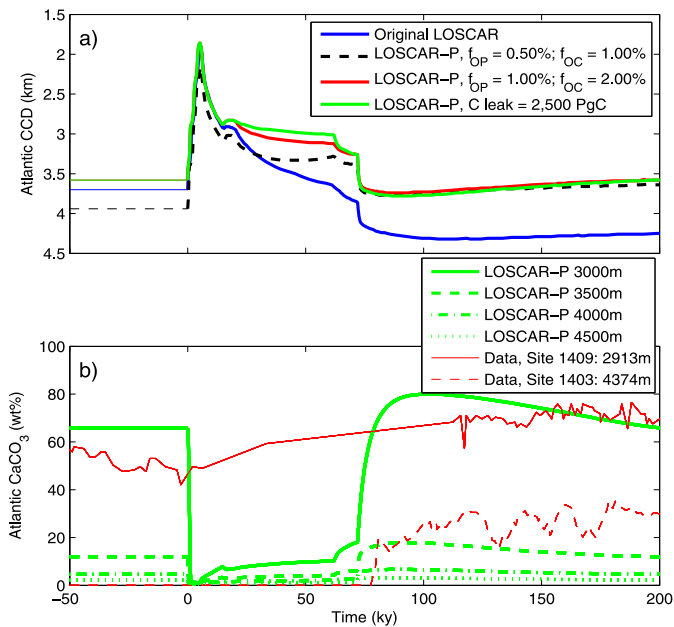


**Fig. 6.** CCD and sediment  $\text{CaCO}_3$  wt% evolution in the Atlantic ocean (corresponding to runs shown in Fig. 5). a) Atlantic CCD. b) Atlantic  $\text{CaCO}_3$  content of the 3000, 3500, 4000, and 4500 m sediment boxes for the “stronger leak” scenario (green line in panel “a”; leak = 2,500 Pg C). Red lines are  $\text{CaCO}_3$  weight content data from Penman et al. (2016). (For interpretation of the references to color in this figure legend, the reader is referred to the web version of this article.)

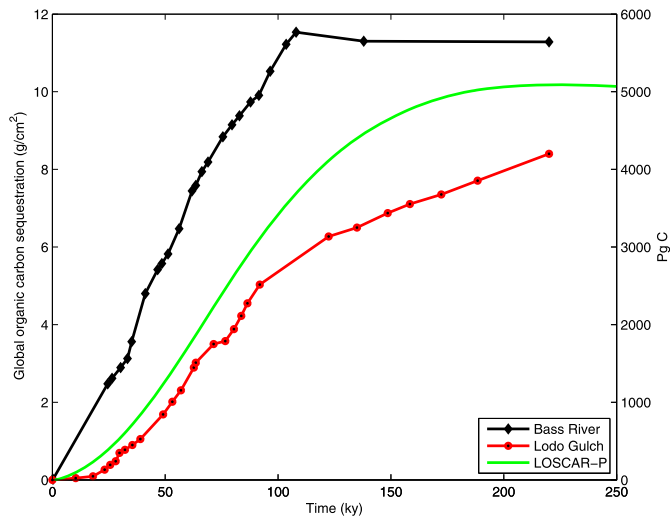


**Fig. 7.** Excess cumulative burial of organic carbon. The black and red lines represent data collected from Bass River and Lodo Gulch, respectively (data from John et al. (2008) that they used to calculate upper and lower global organic C burial across the PETM). The green line is the cumulative accumulation rate of organic C predicted by LOSCAR-P preferred scenario, assuming the continental shelf area of Eocene was twice that of present day. Present day shelf area =  $26 \times 10^9 \text{ km}^2$  (Walsh et al., 1991). (For interpretation of the references to color in this figure legend, the reader is referred to the web version of this article.)

crease in carbonate content in the recovery stage of the PETM are present in LOSCAR-P simulations that have high initial C and P burial fluxes (Fig. 6, solid red and green lines). Nevertheless, for the same carbon input scenario and the same weathering feedback the over-deepening of the CCD in LOSCAR-P is muted compared to that of the original LOSCAR (Fig. 6). The CCD muting in LOSCAR-P arises as a result of the increased phosphate concentration in the surface ocean. Higher  $\text{PO}_4$  concentration yields higher organic carbon export and since the ratio between organic C rain and  $\text{CaCO}_3$  is fixed in LOSCAR, the  $\text{CaCO}_3$  rain to the sediments also increases. Because

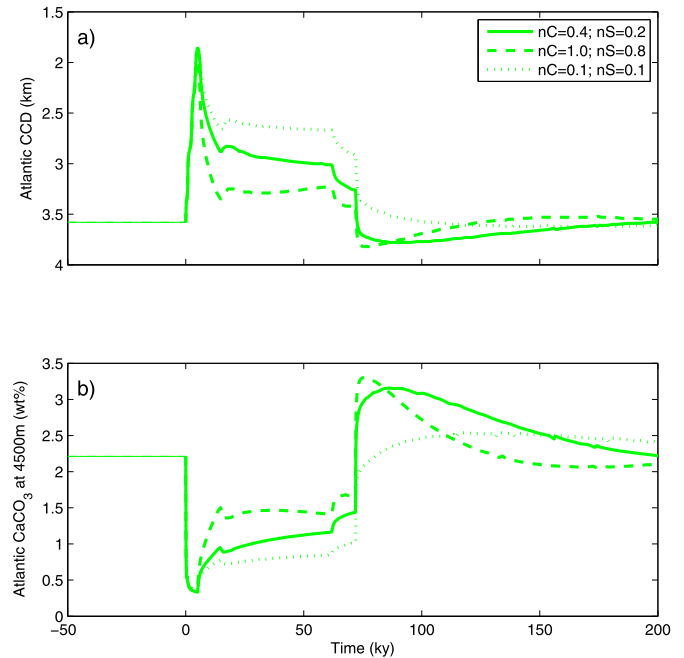


**Fig. 8.** Sensitivity of LOSCAR-P to the weathering feedback strength. Each of the simulation has the same carbon input scenario, which is identical to the “stronger leak” scenario displayed in Figs. 5 and 6. nC and nS are carbonate and silicate weathering feedback parameters, respectively. nC and nS are by default set to 0.4 and 0.2, respectively, and the default value is used in all other simulations. a) Atlantic CCD sensitivity to the weathering feedback strength. b) Atlantic  $\text{CaCO}_3$  content in sediments at depth of 4500 m and its sensitivity to the weathering feedback strength.

the flux of  $\text{CaCO}_3$  per unit area is now larger, the CCD does not have to deepen as much (or at all) in order to balance the riverine input, hence the deepening is not as prominent or completely absent. It is important to mention that the magnitude of the CCD overshoot in the model also depends on the strength of the weathering feedback, which itself is uncertain. The same simulation with a different weathering feedback strength (which is within the uncertainty envelope) could produce a scenario in which there is no CCD overshoot or a scenario with a more pronounced deepening (Fig. 8). However, even when a strong weathering feedback is employed, the CCD over-deepening is not as prominent as indicated by the North Atlantic data.

LOSCAR-P produces a  $\text{CaCO}_3$  content overshoot in the Atlantic ocean at both corresponding depths (which approximate sites U1403 and U1409, see below) but the overshoot at the deeper sediment box (4,500 m, which approximates site 1403) greatly underestimates the data (Fig. 6b). The carbonate content at the deeper site (Site 1403: 4374 m) is elevated by more than 20% around 70 ky after the onset of the PETM. This indicates that the CCD during the termination stage of the PETM likely reached below 4400 meters (at least in the North Atlantic). In contrast, LOSCAR-P produces only a 1% increase in carbonate content during the recovery in the Atlantic sediments box located at 4,500 m. Such a small increase is a result of the muted CCD signal as explained above (the CCD in LOSCAR-P is never deeper than 3,800 m). However, the deep Atlantic in LOSCAR is presented as a single box (i.e. extremely coarse spatial resolution). Therefore, the interpretation of LOSCAR results and their comparison to the data from a specific region should be taken with caution. Thus, we show the response of two additional sediment boxes in the model, between the depths of 3,000 m and 4,500 m, which exhibit an increase in carbonate content during the recovery stage of the PETM of 6% and 2%, at 3,500 m and 4,000 m sediment boxes, respectively, also indicating a slight overshoot but still underestimating the actual data.

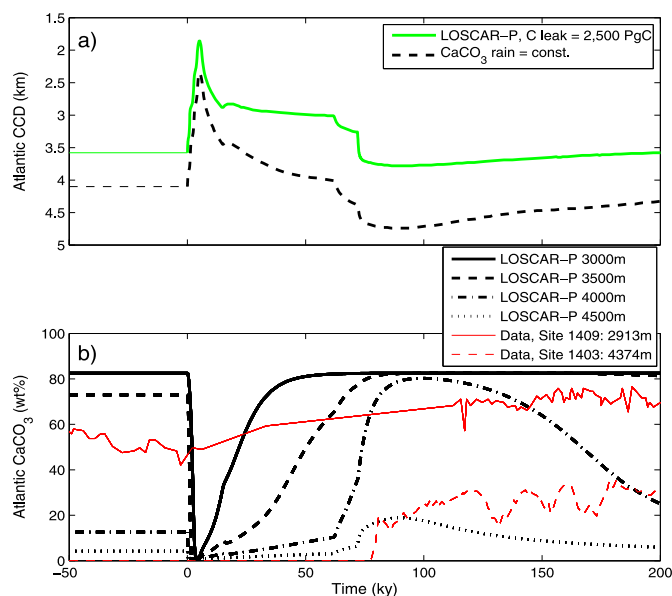


**Fig. 9.** CCD and sediment  $\text{CaCO}_3$  wt% sensitivity to  $\text{CaCO}_3$  rain. Green line represents the preferred scenario, C leak = 2,500 Pg C. Black lines represent a scenario in which  $\text{CaCO}_3$  is kept constant at the initial value. a) Atlantic CCD. b) Atlantic  $\text{CaCO}_3$  content of the 3000, 3500, 4000, and 4500 m sediment boxes for the “stronger leak” scenario. Red lines are  $\text{CaCO}_3$  weight content data from Penman et al. (2016). (For interpretation of the references to color in this figure legend, the reader is referred to the web version of this article.)

Until more sediment sections are recovered from different regions that were positioned below the CCD prior to the PETM, there is no way of knowing for certain if the overshoot was a global event, nor is it possible to know the extent and the magnitude of over-deepening (Penman et al., 2016), which would help validate the model results. If the overshoot was indeed global and of similar magnitude as observed in the North Atlantic ocean (which is very likely), then it would be difficult to reconcile the rapid recovery by an enhanced marine sequestration of organic carbon without assuming a constant (or decreased)  $\text{CaCO}_3$  and alkalinity export during the recovery-stage of the PETM. Note that when such an assumption is invoked, as was the case in the original LOSCAR (Penman et al., 2016), the CCD and  $\text{CaCO}_3$  overshoot is more consistent with the data than the one produced in LOSCAR-P. This is because in simulations performed by Penman et al. (2016) the  $\text{PO}_4$  concentration remains constant throughout the entire model run and therefore the  $\text{CaCO}_3$  rain also stays unchanged, resulting in a deeper CCD (the mechanism explained above) during the recovery phase. Additionally, their initial CCD depth is around 600–700 m deeper than in LOSCAR-P, which contributes to a more pronounced  $\text{CaCO}_3$  overshoot at the 4,500 m sediment box.

To show the effect of  $\text{CaCO}_3$  rain on the CCD and  $\text{CaCO}_3$  content overshoot we ran our preferred carbon emission scenario with the  $\text{CaCO}_3$  rain constant (Fig. 9). We additionally slightly reduce the initial  $\text{CaCO}_3$  rain in order to get an initially deeper CCD, to be more consistent with the Penman et al. (2016) simulations. The constant  $\text{CaCO}_3$  rain scenario yields a more pronounced CCD over-deepening and a stronger  $\text{CaCO}_3$  content overshoot. The 4,500 m sediment box produces an overshoot of 15% during the recovery stage, which is more consistent with the data (Fig. 9, dotted-black line).

The question is whether the constant  $\text{CaCO}_3$  rain assumed in the original LOSCAR or the increasing  $\text{CaCO}_3$  rain predicted by LOSCAR-P is more representative of reality. Gibbs et al. (2010) reconstructed calcareous nannoplankton production at ODP Sites 690, 1209 and Bass River based on nannoplankton counts coupled with taxon-specific Sr/Ca data. According to Gibbs et al. (2010),

there was no significant change in biogenic carbonate production during the PETM. If  $\text{CaCO}_3$  rain indeed did not increase during the PETM, and this assumption is incorporated into the model, then LOSCAR-P produces trends consistent with the current available data. As the validity of this scenario depends on the assumption from only one study, the model results should be interpreted with caution. Also, constant  $\text{CaCO}_3$  rain requires decoupling, to some degree, from organic carbon rain.

#### 4.4. LOSCAR sediment module and respiratory-driven carbonate dissolution

It has been suggested that the organic carbon rain and its subsequent oxidation near the sediment surface might also promote calcium carbonate dissolution within the sediments (even if the bottom water is super-saturated) by reducing the saturation state of the porewater (e.g., Archer et al., 1989; Emerson and Archer, 1990). This respiratory-driven calcite dissolution has been implemented in some sediment models (e.g. Emerson and Archer, 1990; Archer, 1996; Ridgwell, 2007). LOSCAR, however, does currently not account for the effect of organic carbon respiration on  $\text{CaCO}_3$  dissolution. Here, we argue that the lack of the respiratory-driven dissolution in LOSCAR’s sediment model does not significantly impact the model results.

The two different model types, the respiratory-driven model (e.g. GENIE; Ridgwell, 2007) versus non-respiratory model (e.g. LOSCAR), exhibit different wt%  $\text{CaCO}_3$  and the CCD behavior during the PETM aftermath (Penman et al., 2016). During the PETM recovery, in LOSCAR, the elevated saturation state, and therefore the enhanced carbonate burial (see section 4.3), is accommodated by an increase in the  $\text{CaCO}_3$  content of the deep-sea sediments. The  $\text{CaCO}_3$  content of the shallow sediments, located above the lysocline (e.g. 3000 m depth), however, are already at their maximum carbonate “holding capacity” and therefore the carbonate content of the shallow sediments cannot increase any further. On the other hand, respiratory-driven models such as GENIE, simulate dissolution of  $\text{CaCO}_3$  even in the sediments above the lysocline. The  $\text{CaCO}_3$  depletion of shallow sediments (as observed during the PETM onset and main phase) in such models, caused by organic carbon respiration, increases the potential of those sediments to hold more carbonate during the high saturation events (as observed during the PETM recovery). For those reasons, LOSCAR accommodates the increase in carbonate burial during the recovery-phase of the PETM mainly by increasing the depth of the CCD (compared to the pre-event depth). Whereas respiratory-driven sediment models can accommodate such change in the shallow sediments, thus not producing the CCD over-deepening or the  $\text{CaCO}_3$  overshoot. According to data, both mechanisms or the combination of the two may be representative of the real world (Penman et al., 2016).

The respiratory-driven sediment models suggest that the rate of  $\text{CaCO}_3$  accumulation/dissolution in the deep sea depends heavily on the ratio between the organic carbon and calcium carbonate carbon reaching the sediments (rain ratio) (Emerson and Archer, 1990; Archer, 1991, 1996). It is important to note that there is very little difference in predicted lysocline response between the rain ratio of 0 (essentially no organic carbon reaching the sediments) and rain ratio of 0.5 model scenarios (see Figure 5 in Archer, 1991). When this rain ratio is low (org./inorg. < 0.5) the calcite dry content in the sediments is not greatly affected by organic carbon respiration above the saturation horizon (Archer, 1991). Even in slightly undersaturated waters (just below the saturation horizon) the rate of  $\text{CaCO}_3$  accumulation is not significantly altered by organic carbon respiration when the organic to inorganic carbon rain ratio is low (Archer, 1991). We examined the amounts of organic and inorganic carbon reaching the sediments in LOSCAR at the rel-

evant depth (4,000 m; see below) in order to determine whether the absence of the respiratory-driven sediment model would significantly alter the results of this study.

Because the CCD in LOSCAR during the recovery phase of the PETM is around 4,000 m, which is in good agreement with the CCD reconstructed from data (Slotnick et al., 2015), and because the paleodepth of the sediment core recovered from site U1403 was around 4,000 m, we define this as the depth of interest. The organic carbon flux from the surface ocean is attenuated with depth, thus knowing the export flux of organic carbon at the surface allows for approximation of the flux at any ocean depth using, e.g., the Martin curve (Martin et al., 1987):

$$F = F_{100} \times \left( \frac{z}{100} \right)^{-b} \quad (8)$$

where  $F$  is the organic carbon flux at the depth  $z$  (m) and  $F_{100}$  is the particulate organic carbon export at 100 m, and  $b$  is the attenuation factor with the standard value of 0.858 (Martin et al., 1987).

According to the Martin curve, about 4% of the organic carbon production in the surface ocean reaches the depth of 4,000 m. In the default LOSCAR-P simulation this translates to  $\sim 0.05 \text{ mol C m}^{-2} \text{ yr}^{-1}$  in the low latitude ocean. The revisited carbon flux study for the modern ocean suggests that the attenuation factor in warmer waters (among other factors), at the Hawaii Ocean time series, can be as high as 1.33 (Buesseler et al., 2007), meaning that only 0.7% ( $\sim 0.008 \text{ mol C m}^{-2} \text{ yr}^{-1}$  in LOSCAR) of the surface ocean production could be reaching the depth of 4,000 m. Total inorganic carbon rain to sediments in LOSCAR is around  $0.11 \text{ mol C m}^{-2} \text{ yr}^{-1}$  ( $40 \times 10^{12} \text{ mol C yr}^{-1}$ , comparable to the modern day value of  $32 \times 10^{12} \text{ mol C yr}^{-1}$  Milliman, 1993), and specifically in the Atlantic ocean at 4,000 m depth is  $\sim 0.10 \text{ mol C m}^{-2} \text{ yr}^{-1}$ . Thus, the standard Martin curve produces a rain ratio of 0.5 in LOSCAR's deep ocean. The Martin curve with strong attenuation, pertaining to a subtropical gyre yields even a smaller ratio ( $\sim 0.1$  for  $b = 1.33$ ) of organic to inorganic C. The revised Martin curve study was based on the export flux measurements from two different environments. One located in colder waters in the Northwest Pacific subarctic gyre, and the other located in warm waters north of a subtropical gyre north of Hawaii. The stronger attenuation factor ( $b = 1.33$ ) belongs to the warmer site, while the colder locality showed a significantly weaker attenuation with depth ( $b = 0.51$ ) (Buesseler et al., 2007). In the modern ocean, the majority of organic carbon export to the deep sediments takes place within 30 degrees of the equator (Jahnke, 1996), meaning that the globally averaged attenuation factor in the Martin curve should be skewed towards the higher value. It has been argued that the export flux differences between the two sites might have arisen due to different heterotrophic metabolic rates, influenced by contrasting water temperatures (Olivarez Lyle and Lyle, 2006; Buesseler et al., 2007; Matsumoto, 2007). If this is in fact the reason, then due to warmer global temperatures during the PETM the Martin curve for the modern ocean subtropical region ( $b = 1.33$ ) is more representative of the mean global organic carbon export attenuation during the PETM. In that case, the  $\text{CaCO}_3$  dissolution caused by organic carbon respiration would be even more diminished. As stated above, for Corg/ $\text{CaCO}_3$  ratios  $< 0.5$ , respiratory-driven dissolution is essentially negligible (Archer, 1991).

Even if respiratory-driven dissolution was important during the PETM, would the respiration rate significantly change for varying phosphate concentration and organic carbon export in our model scenarios? It turns out that even though the carbon export in LOSCAR increases with time (Fig. 2b), respiration does not change significantly. It decreases by less than 1% at the peak carbon export. This is due to the fact that an increase in carbon export is

accompanied by an increase in organic carbon burial, thus the difference between the two is nearly constant. In summary, because of the relatively constant respiration rate and a low ratio of organic to inorganic carbon reaching the deep sediments our, CCD over-deepening and  $\text{CaCO}_3$  sediment weight content overshoot results can be used as a model constraint, even though the model is lacking respiratory-driven carbonate dissolution in the sediments.

## 5. Summary and conclusions

The Paleocene–Eocene Thermal Maximum ( $\sim 56 \text{ Ma}$ ) was an event characterized by a major carbon cycle perturbation manifested in the geological record as a large negative  $\delta^{13}\text{C}$  excursion (e.g., McInerney and Wing, 2011), global warming of more than  $5^\circ\text{C}$  (as inferred from  $\delta^{18}\text{O}$  isotopes) (Zachos et al., 2003; Tripati et al., 2009), and severe dissolution of carbonate sediments (e.g., Zachos et al., 2005). These anomalies can collectively only be generated by a large and rapid introduction of carbon into the ocean–atmosphere system. As such, the PETM is considered the most important analog to the ongoing anthropogenic carbon emissions and thus has been intensively studied. The majority of the studies were focused on resolving the source and the magnitude of carbon input (onset phase) (e.g., Dickens et al., 1995; Zachos et al., 2005; Zeebe et al., 2009), as well as the duration of the emissions (onset + main phase) (e.g., Zeebe et al., 2016) or the event as a whole (e.g., Farley and Eltgroth, 2003; Murphy et al., 2010; Röhl et al., 2007), while relatively few studies were centered around the recovery-stage of the PETM (Bowen and Zachos, 2010).

Here, we primarily focus on the termination stage of the PETM and the mechanisms responsible for restoration of the earth–ocean system biogeochemistry after a major carbon perturbation. We show that a coupled carbon–phosphorus model with a redox-controlled reactive P and organic C burial produces enhanced carbon sequestration during the PETM. The total amount of carbon sequestered is independent of the locale (Atlantic ocean vs. atmosphere) of the simulated methane oxidation (see Supplement). In order to explain the accelerated  $\delta^{13}\text{C}$  restoration during the recovery-phase of the PETM a larger initial throughput of P is required, resulting in the residence time of dissolved phosphate in the ocean of  $\sim 21 \text{ ky}$ , which is within the range estimated for the modern ocean (16 ky–38 ky; Ruttenberg, 1993).

Our preferred scenario produces trends consistent with oxygen (e.g., Chun et al., 2010; Dickson et al., 2012; Pälike et al., 2014; Sluijs et al., 2014), excess accumulation rates of organic carbon (John et al., 2008), export production (Bains et al., 2000; Ma et al., 2014), sediment carbonate content (Penman et al., 2016) and  $\delta^{13}\text{C}$  data. Unlike Bowen and Zachos (2010), we do not assume an ad-hoc, transient increase in organic carbon burial. The burial is rather predicted and driven by the redox-dependency between organic carbon and phosphorus. However, the standard LOSCAR-P model fails to quantitatively recreate the magnitude of the CCD and carbonate content overshoot observed in the North Atlantic as the model mutes the overshoot signal by predicting an increase in carbonate rain from the surface ocean. The accelerated earth-system biogeochemical recovery during the PETM could be ascribed to the rise in nutrient supply and enhanced primary production and consequential increase in organic carbon sequestration only if the  $\text{CaCO}_3$  rain remained constant (or decreased) during the termination stage of the PETM.

## Acknowledgements

This research was supported by an NSF subaward of OCE13-38842 and OCE16-58023 to R.E.Z.

## Appendix A. Supplementary material

Supplementary material related to this article can be found online at <https://doi.org/10.1016/j.epsl.2017.09.011>.

## References

- Archer, D., 1991. Modeling the calcite lysocline. *J. Geophys. Res.* 96, 17037–17050.
- Archer, D., 1996. A data-driven model of the global calcite lysocline. *Glob. Biogeochem. Cycles* 10 (3), 511–526.
- Archer, D., Emerson, S., Reimers, C., 1989. Dissolution of calcite in deep-sea sediments: pH and O<sub>2</sub> microelectrode results. *Geochim. Cosmochim. Acta* 53 (11), 2831–2845.
- Bains, S., Norris, R.D., Corfield, R.M., Faul, K.L., 2000. Termination of global warmth at the Palaeocene/Eocene boundary through productivity feedback. *Nature* 407 (6801), 171–174.
- Bice, K.L., Barron, E.J., Peterson, W.H., 1998. Reconstruction of realistic Early Eocene Paleobathymetry and Ocean GCM sensitivity to specified basin configuration. In: Crowley, T.J., Burke, K.C. (Eds.), *Tectonic Boundary Conditions for Climate Reconstructions*. Oxford University Press, pp. 227–247.
- Bowen, G.J., 2013. Up in smoke: a role for organic carbon feedbacks in Paleogene hyperthermals. *Glob. Planet. Change* 109, 18–29.
- Bowen, G.J., Zachos, J.C., 2010. Rapid carbon sequestration at the termination of the Palaeocene–Eocene thermal maximum. *Nat. Geosci.* 3 (12), 866–869.
- Broecker, W.S., 1982. Ocean chemistry during glacial times. *Geochim. Cosmochim. Acta* 46, 1689–1705.
- Buesseler, K.O., Lamborg, C.H., Boyd, P.W., Lam, P.J., Trull, T.W., Bidigare, R.R., Bishop, J.K., Casciotti, K.L., Dehairs, F., Elskens, M., et al., 2007. Revisiting carbon flux through the ocean's twilight zone. *Science* 316 (5824), 567–570.
- Chun, C.O., Delaney, M.L., Zachos, J.C. Paleoredox changes across the Paleocene–Eocene thermal maximum, Walvis Ridge (ODP Sites 1262, 1263, and 1266): evidence from Mn and U enrichment factors. *Paleoceanography* 25 (4).
- DeConto, R.M., Galeotti, S., Pagani, M., Tracy, D., Schaefer, K., Zhang, T., Pollard, D., Beerling, D.J., 2012. Past extreme warming events linked to massive carbon release from thawing permafrost. *Nature* 484 (7392), 87–91.
- Dickens, G.R., 2001. Carbon addition and removal during the Late Palaeocene Thermal Maximum: basic theory with a preliminary treatment of the isotope record at ODP Site 1051, Blake Nose. In: Kroon, D., Norris, R.D., Klaus, A. (Eds.), *Western North Atlantic Palaeogene and Cretaceous Palaeoceanography*, vol. 183. Geol. Soc. London. Special Publication, pp. 293–305.
- Dickens, G.R., 2003. Rethinking the global carbon cycle with a large, dynamic and microbially mediated gas hydrate capacitor. *Earth Planet. Sci. Lett.* 213, 169–183.
- Dickens, G.R., O'Neil, J.R., Rea, D.K., Owen, R.M., 1995. Dissociation of oceanic methane hydrate as a cause of the carbon isotope excursion at the end of the Paleocene. *Paleoceanography* 10, 965–971.
- Dickens, G.R., Castillo, M.M., Walker, J.C.G., 1997. A blast of gas in the latest Paleocene; simulating first-order effects of massive dissociation of oceanic methane hydrate. *Geology* 25, 259–262.
- Dickson, A.J., Cohen, A.S., Coe, A.L., 2012. Seawater oxygenation during the Paleocene–Eocene thermal maximum. *Geology* 40 (7), 639–642.
- Dickson, A.J., Rees-Owen, R.L., März, C., Coe, A.L., Cohen, A.S., Pancost, R.D., Taylor, K., Shcherbinina, E., 2014. The spread of marine anoxia on the northern Tethys margin during the Paleocene–Eocene Thermal Maximum. *Paleoceanography* 29 (6), 471–488.
- Emerson, S., Archer, D., 1990. Calcium carbonate preservation in the ocean. *Philos. Trans. R. Soc., Math. Phys. Eng. Sci.* 331 (1616), 29–40.
- Farley, K.A., Eltgroth, S.F., 2003. An alternative age model for the Paleocene–Eocene thermal maximum using extraterrestrial <sup>3</sup>He. *Earth Planet. Sci. Lett.* 208, 135–148.
- Filippelli, G.M., 2001. Carbon and phosphorus cycling in anoxic sediments of the Saanich Inlet, British Columbia. *Mar. Geol.* 174 (1), 307–321.
- Flögel, S., Wallmann, K., Poulsen, C., Zhou, J., Oschlies, A., Voigt, S., Kuhnt, W., 2011. Simulating the biogeochemical effects of volcanic CO<sub>2</sub> degassing on the oxygenate state of the deep ocean during the Cenomanian/Turonian Anoxic Event (OAE2). *Earth Planet. Sci. Lett.* 305 (3), 371–384.
- Gibbs, S.J., Bralower, T.J., Bown, P.R., Zachos, J.C., Bybell, L.M., 2006. Shelf and open-ocean calcareous phytoplankton assemblages across the Paleocene–Eocene Thermal Maximum: implications for global productivity gradients. *Geology* 34 (4), 233–236.
- Gibbs, S.J., Stoll, H.M., Bown, P.R., Bralower, T.J., 2010. Ocean acidification and surface water carbonate production across the Paleocene–Eocene thermal maximum. *Earth Planet. Sci. Lett.* 295 (3), 583–592.
- Hartnett, H.E., Keil, R.G., Hedges, J.I., Devol, A.H., 1998. Influence of oxygen exposure time on organic carbon preservation in continental margin sediments. *Nature* 391 (6667), 572–575.
- Ingall, E.D., Bustin, R., Van Cappellen, P., 1993. Influence of water column anoxia on the burial and preservation of carbon and phosphorus in marine shales. *Geochim. Cosmochim. Acta* 57 (2), 303–316.
- Jahnke, R.A., 1996. The global ocean flux of particulate organic carbon: areal distribution and magnitude. *Glob. Biogeochem. Cycles* 10 (1), 71–88.
- John, C.M., Bohaty, S.M., Zachos, J.C., Sluijs, A., Gibbs, S., Brinkhuis, H., Bralower, T.J. North American continental margin records of the Paleocene–Eocene thermal maximum: implications for global carbon and hydrological cycling. *Paleoceanography* 23 (2).
- Kelly, D.C., Zachos, J.C., Bralower, T.J., Schellenberg, S.A., 2005. Enhanced terrestrial weathering/runoff and surface-ocean carbonate production during the recovery stages of the Paleocene–Eocene Thermal Maximum. *Paleoceanography* 20, PA4023. <http://dx.doi.org/10.1029/2005PA001163>.
- Kelly, D.C., Nielsen, T.M., McCarren, H.K., Zachos, J.C., Röhl, U., 2010. Spatiotemporal patterns of carbonate sedimentation in the South Atlantic: implications for carbon cycling during the Paleocene–Eocene thermal maximum. *Palaeogeogr. Palaeoclimatol. Palaeoecol.* 293 (1), 30–40.
- Kennett, J.P., Stott, L.D., 1991. Abrupt deep-sea warming, palaeoceanographic changes and benthic extinctions at the end of the Palaeocene. *Nature* 353, 225–229.
- Komar, N., Zeebe, R., 2016. Calcium and calcium isotope changes during carbon cycle perturbations at the end-Permian. *Paleoceanography* 31 (1), 115–130.
- Komar, N., Zeebe, R., Dickens, G., 2013. Understanding long-term carbon cycle trends: the late Paleocene through the early Eocene. *Paleoceanography* 28 (4), 650–662.
- Kurtz, A., Kump, L.R., Arthur, M.A., Zachos, J.C., Paytan, A., 2003. Early Cenozoic decoupling of the global carbon and sulfur cycles. *Paleoceanography* 18, 1090.
- Lenton, T.M., Watson, A.J., 2000. Redfield revisited, 1: regulation of nitrate, phosphate, and oxygen in the ocean. *Glob. Biogeochem. Cycles* 14 (1), 225–248.
- Leon-Rodriguez, L., Dickens, G.R., 2010. Constraints on ocean acidification associated with rapid and massive carbon injections: the early Paleogene record at ocean drilling program site 1215, equatorial Pacific Ocean. *Palaeogeogr. Palaeoclimatol. Palaeoecol.* 298, 409–420.
- Ma, Z., Gray, E., Thomas, E., Murphy, B., Zachos, J., Paytan, A., 2014. Carbon sequestration during the Palaeocene–Eocene Thermal Maximum by an efficient biological pump. *Nat. Geosci.* 7 (5), 382–388.
- Martin, J.H., Knauer, G.A., Karl, D.M., Broenkow, W.W., 1987. VERTEX: carbon cycling in the northeast Pacific. *Deep-Sea Res.* 34 (2), 267–285.
- Matsumoto, K. Biology-mediated temperature control on atmospheric pCO<sub>2</sub> and ocean biogeochemistry. *Geophysical Research Letters* 34 (20).
- McInerney, F.A., Wing, S.L., 2011. The Paleocene–Eocene Thermal Maximum: a perturbation of carbon cycle, climate, and biosphere with implications for the future. *Annu. Rev. Earth Planet. Sci.* 39, 489–516.
- Milliman, J.D., 1993. Production and accumulation of calcium carbonate in the ocean: Budget of a nonsteady state. *Glob. Biogeochem. Cycles* 4, 927–957.
- Murphy, B., Farley, K., Zachos, J., 2010. An extraterrestrial 3 He-based timescale for the Paleocene–Eocene thermal maximum (PETM) from Walvis Ridge, IODP Site 1266. *Geochim. Cosmochim. Acta* 74 (17), 5098–5108.
- Olivarez Lyle, A., Lyle, M.W., 2006. Missing organic carbon in Eocene marine sediments: is metabolism the biological feedback that maintains end-member climates. *Paleoceanography* 21, PA2007. <http://dx.doi.org/10.1029/2005PA001230>.
- Pagani, M., Calderia, K., Archer, D., Zachos, J.C., 2006. An ancient carbon mystery. *Science* 314, 1556–1557.
- Pälike, C., Delaney, M.L., Zachos, J.C., 2014. Deep-sea redox across the Paleocene–Eocene thermal maximum. *Geochim. Geophys. Res.* 15 (4), 1038–1053.
- Pancost, R.D., Steart, D.S., Handley, L., Collinson, M.E., Hooker, J.J., Scott, A.C., Grassineau, N.V., Glasspool, I.J., 2007. Increased terrestrial methane cycling at the Paleocene–Eocene thermal maximum. *Nature* 449 (7160), 332–335.
- Penman, D.E., 2016. Silicate weathering and North Atlantic silica burial during the Paleocene–Eocene Thermal Maximum. *Geology*, G37704-1.
- Penman, D.E., Turner, S.K., Sexton, P.F., Norris, R.D., Dickson, A.J., Boulila, S., Ridgwell, A., Zeebe, R.E., Zachos, J.C., Cameron, A., et al. An abyssal carbonate compensation depth overshoot in the aftermath of the Palaeocene–Eocene Thermal Maximum. *Nature Geoscience*.
- Ravizza, G., Norris, R.N., Blusztajn, J., Aubry, M.-P., 2001. An osmium isotope excursion associated with the late Paleocene thermal maximum: evidence of intensified chemical weathering. *Paleoceanography* 16, 155–163.
- Ridgwell, A. Interpreting transient carbonate compensation depth changes by marine sediment core modeling. *Paleoceanography* 22 (4).
- Röhl, U., Westerhold, T., Bralower, T.J., Zachos, J.C. On the duration of the Paleocene–Eocene thermal maximum (PETM). *Geochemistry, Geophysics, Geosystems* 8 (12).
- Ruttenberg, K., 1993. Reassessment of the oceanic residence time of phosphorus. *Chem. Geol.* 107 (3–4), 405–409.
- Schulte, P., Scheibner, C., Speijer, R.P., 2011. Fluvial discharge and sea-level changes controlling black shale deposition during the Paleocene–Eocene Thermal Maximum in the Dababiya Quarry section, Egypt. *Chem. Geol.* 285 (1), 167–183.
- Slomp, C., Van Cappellen, P., 2007. The global marine phosphorus cycle: sensitivity to oceanic circulation. *Biogeosciences* 4, 155–171.
- Slotnick, B.S., Lauretano, V., Backman, J., Dickens, G.R., Sluijs, A., Lourens, L., 2015. Early Paleogene variations in the calcite compensation depth: new constraints using old borehole sediments from across Ninetyeast Ridge, central Indian Ocean. *Clim. Past* 11, 473–493.

- Sluijs, A., Schouten, S., Pagani, M., Woltering, M., Brinkhuis, H., Damste, J.S.S., Dickens, G.R., Huber, M., Reichert, G., Stein, R., Mattheissen, J., Lourens, L.J., Pedentchouk, N., Backman, J., Moran, K., 2006. Subtropical Arctic Ocean temperatures during the Palaeocene/Eocene thermal maximum. *Nature* 441, 610–613.
- Sluijs, A., Brinkhuis, H., et al., 2009. A dynamic climate and ecosystem state during the Paleocene–Eocene Thermal Maximum: inferences from dinoflagellate cyst assemblages on the New Jersey Shelf. *Biogeosciences* 6 (8), 1755–1781.
- Sluijs, A., Van Rooij, L., Harrington, G., Schouten, S., Sessa, J., LeVay, L., Reichert, G.-J., Slomp, C., 2014. Warming, euxinia and sea level rise during the Paleocene–Eocene Thermal Maximum on the Gulf Coastal Plain: implications for ocean oxygenation and nutrient cycling. *Clim. Past* 10 (4), 1421–1439.
- Stoll, H.M., Bains, S. Coccolith Sr/Ca records of productivity during the Paleocene–Eocene thermal maximum from the Weddell Sea. *Paleoceanography* 18 (2).
- Svensen, H., Planke, S., Malthes-Sørensen, A., Jamtveit, B., Myklebust, R., Eidem, T.R., Rey, S.S., 2004. Release of methane from a volcanic basin as a mechanism for initial Eocene global warming. *Nature* 429 (6991), 542–545.
- Takahashi, Taro, Broecker, Wallace S., Langer, Sara, 1985. Redfield ratio based on chemical data from isopycnal surfaces. *J. Geophys. Res. Oceans* 90 (C4), 6907–6924.
- Tripati, A., Roberts, C.D., Eagle, R.E., 2009. Coupling of CO<sub>2</sub> and ice sheet stability over major climate transitions of the last 20 million years. *Sci. Express*. <http://dx.doi.org/10.1126/science.1178296>.
- Tsandeov, I., Slomp, C., 2009. Modeling phosphorus cycling and carbon burial during Cretaceous Oceanic Anoxic Events. *Earth Planet. Sci. Lett.* 286 (1), 71–79.
- Tyrrell, T., 1999. The relative influences of nitrogen and phosphorus on oceanic primary production. *Nature* 400 (6744), 525–531.
- Uchikawa, J., Zeebe, R.E., 2008. Influence of terrestrial weathering on ocean acidification and the next glacial inception. *Geophys. Res. Lett.* 35, L23608. <http://dx.doi.org/10.1029/2008GL035963>.
- Van Cappellen, P., Ingall, E.D., 1994. Benthic phosphorus regeneration, net primary production, and ocean anoxia: a model of the coupled marine biogeochemical cycles of carbon and phosphorus. *Paleoceanography* 9 (5), 677–692.
- Wallmann, K., 2003. Feedbacks between oceanic redox states and marine productivity: a model perspective focused on benthic phosphorus cycling. *Glob. Biogeochem. Cycles* 17 (3).
- Wallmann, K., 2010. Phosphorus imbalance in the global ocean? *Glob. Biogeochem. Cycles* 24 (4).
- Walsh, J.J., Biscaye, P., Csanady, G., 1991. Importance of continental margins in the marine biogeochemical cycling of carbon and nitrogen. *Nature* 350 (6313), 53–55.
- Weiss, R., 1970. The solubility of nitrogen, oxygen and argon in water and seawater. In: *Deep-Sea Res. Oceanogr. Abstr.*, vol. 17. Elsevier, pp. 721–735.
- Wolf-Gladrow, D.A., Zeebe, R.E., Klaas, C., Körtzinger, A., Dickson, A.G., 2007. Total alkalinity: the explicit conservative expression and its application to biogeochemical processes. *Mar. Chem.* 106 (1), 287–300.
- Zachos, J.C., Wara, M.W., Bohaty, S., Delaney, M.L., Petrizzo, M.R., Brill, A., Bralower, T.J., Premoli-Silva, I., 2003. A transient rise in tropical sea surface temperature during the Paleocene–Eocene thermal maximum. *Science* 302, 1551–1554.
- Zachos, J.C., Röhl, U., Schellenberg, S.A., Sluijs, A., Hodell, D.A., Kelly, D.C., Thomas, E., Nicoloa, M., Raffi, I., Lourens, L.J., McCarren, H., Kroon, D., 2005. Rapid acidification of the ocean during the Paleocene–Eocene thermal maximum. *Science* 308, 1611–1615.
- Zachos, J.C., Dickens, G.R., Zeebe, R.E., 2008. An early Cenozoic perspective on greenhouse warming and carbon-cycle dynamics. *Nature* 451, 279–283. <http://dx.doi.org/10.1038/nature06588>.
- Zeebe, R.E., 2012. LOSCAR: Long-term Ocean–atmosphere–Sediment Carbon cycle Reservoir Model v2.0.4. *Geosci. Model Dev.* 1, 149–166.
- Zeebe, R.E., Wolf-Gladrow, D.A., 2001. CO<sub>2</sub> in Seawater: Equilibrium, Kinetics, Isotopes. Elsevier Oceanography Series, Amsterdam, p. 346.
- Zeebe, R.E., Zachos, J.C., 2013. Long-term legacy of massive carbon input to the Earth system: Anthropocene versus Eocene. *Philos. Trans. R. Soc., Math. Phys. Eng. Sci.* 371 (2001), 20120006.
- Zeebe, R.E., Zachos, J.C., Caldeira, K., Tyrrell, T., 2008. Oceans: carbon emissions and acidification (in perspectives). *Science* 321, 51–52. <http://dx.doi.org/10.1126/science.1159124>.
- Zeebe, R.E., Zachos, J.C., Dickens, G.R., 2009. Carbon dioxide forcing alone insufficient to explain Palaeocene–Eocene Thermal Maximum warming. *Nat. Geosci.* published online: 13 July 2009 <https://doi.org/10.1038/NGEO578>.
- Zeebe, R.E., Ridgwell, A., Zachos, J.C., 2016. Anthropogenic carbon release rate unprecedented during the past 66 million years. *Nat. Geosci.* 9 (4), 325–329.